



Power Electronic Systems
Laboratory

© 2011 IEEE

Proceedings of the IEEE Energy Conversion Congress and Exposition (ECCE USA 2011), Phoenix, USA,
September 18-22, 2011.

Design Study for Exterior Rotor Bearingless Permanent Magnet Machines

T. Reichert
T. Nussbaumer
J.W. Kolar

This material is posted here with permission of the IEEE. Such permission of the IEEE does not in any way imply IEEE endorsement of any of ETH Zurich's products or services. Internal or personal use of this material is permitted. However, permission to reprint/republish this material for advertising or promotional purposes or for creating new collective works for resale or redistribution must be obtained from the IEEE by writing to pubs-permissions@ieee.org. By choosing to view this document, you agree to all provisions of the copyright laws protecting it.



Eidgenössische Technische Hochschule Zürich
Swiss Federal Institute of Technology Zurich

Design Study for Exterior Rotor Bearingless Permanent Magnet Machines

Thomas Reichert, Johann W. Kolar
Power Electronic Systems Laboratory
ETH Zurich
Zurich, Switzerland
reichert@lem.ee.ethz.ch

Thomas Nussbaumer
Levitronix GmbH
Zurich, Switzerland

Abstract— This paper describes important design considerations for a bearingless brushless motor in exterior rotor construction. In order to come up with a compact, energy-dense setup which can provide both bearing forces and high torque, several parameters have to be accounted for while considering mutual dependencies. Moreover, the magnetic bearing and the drive are interlinked for this disk-shaped bearingless motor (with combined concentrated windings). A detailed analysis about the design of the stator teeth has been undertaken and the influence on torque and active and passive radial forces has been investigated.

Index Terms— Motor design, brushless motor, bearingless motor, self-bearing motor, exterior rotor

I. INTRODUCTION

In various industrial processes of fluid handling, a sealed chamber is required to separate the process liquid from the environment [1],[2]. Especially for high-purity applications or in the case of hazardous process substances, a reliable separation has to be guaranteed. However, most of the processes depend on interactions of the process liquid with its surroundings. One of the most prominent steps in an industrial process is the application of a rotational force to the liquid (e.g. mixing, pumping). For this purpose, the rotational force has to be transmitted into the sealed chamber from an electrical motor outside of the process room. Moreover, the rotational component part inside the process room needs to be supported with some type of bearing.

Several solutions already exist for this application, but they all suffer from certain drawbacks. The rotational force could be passed into the process chamber using a sealed opening. However, no seal is completely leakage-proof, wherefore it is not suitable for hazardous liquids. Moreover, particles are generated that impact high-purity applications. Alternative implementations with magnetic couplings avoid an opening in the process chamber. With this solution however, an additional bearing (usually some type of sliding contact bearing) is required inside the process room, which is unfavorable for high-purity as well. An additional drawback

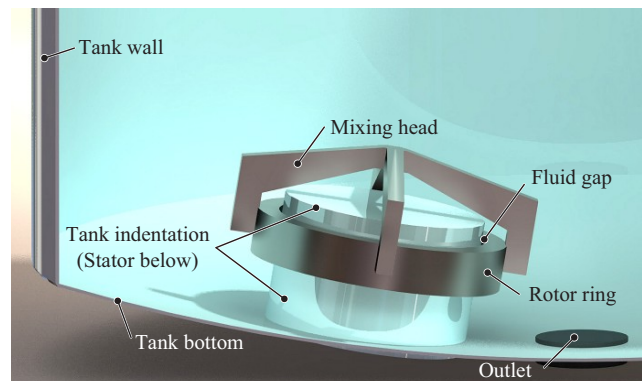


Figure 1. Setup of a bearingless motor with exterior rotor implemented for mixing applications. The stator is buried below a tank indentation. With this measure, only the levitated rotor (with the mixing head) is inside the tank. There is a fluid gap between the rotor ring and the tank indentation.

of both solutions emerges for applications with delicate process liquids, such as bioreactor applications. Seals, magnetic couplings and additional bearings lead to pinch-off areas that can harm the process fluid or solid particles inside the tank (e.g. blood or cell cultures) [3].

With a bearingless brushless motor [4]-[9], all the aforementioned disadvantages can be overcome. This motor type consists of a magnetic bearing, which is integrated into the magnetic circuit of the drive. Therefore, a very compact setup can be achieved and due to the contactless manner of force transmission for both bearing and drive, the problems of particle contamination and pinch-off areas are eliminated. As an additional benefit, the absence of wear promises a longer life time and less maintenance cost.

This paper focuses on a disk-shaped bearingless brushless motor with an exterior rotor (see Fig. 1), with passive stabilization of the axial and the tilting position. The rotor itself is encapsulated and connected with the mixing head. It is the only component that is placed inside the process room. The stator is installed below a tank indentation and connected to the power and control unit outside of the tank. Using this exterior rotor construction type, high torque can be achieved while the rotational speed will be in a moderate range (up to 500 rpm). This bearingless motor is highly qualified for high-purity mixing applications or it can be directly integrated into

a bioreactor, building a bearingless agitator. Such an agitator would reduce cell destruction because of the large magnetic gap resulting in the absence of pinch-off areas. Furthermore, the large magnetic gap facilitates cleaning-in-place and sterilization-in-place applications [10]. Thanks to these benefits, additional implementation costs and an increased control effort are outweighed.

In [11] and [12], the bearingless motor for stirred bioreactors has been introduced and the design optimization for two specific topologies has been undertaken. Moreover, the control of the bearingless motor with concentrated combined windings has been explained. In this paper, the focus lies on a more general design study for this novel and promising motor technology with exterior rotor, as this has not been treated in literature yet. In section II, the design parameters are presented and their interdependencies are discussed. Particular attention is given to the design of the stator teeth and the tooth tips with a detailed analysis presented in section III, where the influence on the torque and the passive and active radial force in dependence on the stator tooth shape is derived and discussed. Finally, in section IV, a test setup is presented.

II. DESIGN PARAMETERS FOR BEARINGLESS MOTORS

The design of a bearingless motor is a complex task because several factors influence each other. Moreover, some of the design goals contradict each other (see section 3). For the targeted application, high torque has to be achieved and high priority is given to this requirement in the design. Additionally, the bearing forces need to be sufficiently large in order to levitate the rotor permanently during operation. For this purpose, both passive reluctance forces as well as active radial bearing forces according to [4] have to be considered in the design.

For the design analysis in this paper, a topology with a stator consisting of six stator teeth has been chosen. It is surrounded by the rotor, which is built of 16 radially magnetized permanent magnets and a back iron ring [12]. The axial and the tilting position are stabilized passively by means of attracting reluctance forces between the stator iron and the rotor magnets. The radial position is also influenced by this passive reluctance force. In this case however, there is no stable working point and an active radial bearing has to be implemented. It is realized with the six concentrated coils and superimposed to the drive control. This means that with all six coils, radial bearing forces and drive torque are generated simultaneously.

Fig. 2 shows the geometric design parameters that define the bearingless motor. There are five parameters that define the radial dimensions. The outer rotor radius r_R determines the overall motor size. The available space is then split into the rotor, the magnetic gap δ_m and the stator inside the hollow rotor. For the rotor, the back iron δ_{BI} and the magnet thicknesses δ_{PM} have to be determined, which will also determine the inner rotor radius. In order to achieve high torque, the rotor should be chosen narrow (leading to a large radius of the magnetic gap, which is the lever arm of the motor). However, the permanent magnets have to provide a

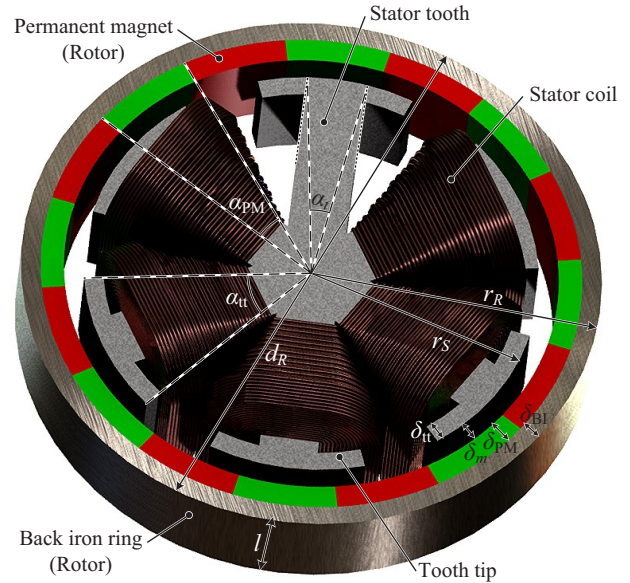


Figure 2. Geometric design parameters of the bearingless brushless motor with a ring-shaped exterior rotor. The exemplary topology consists of six stator teeth and 16 permanent magnets. One coil has been omitted for better visibility.

certain magnetic flux passing through the gap in order to achieve large active and passive forces. Therefore, a certain minimum required magnet thickness (usually in the range of the magnetic gap) is necessary, which then defines the lower limit for the back iron thickness in order to avoid saturation of the iron. If the inner rotor radius is set, either the magnetic gap thickness or the outer stator radius r_S can be chosen, because these values now depend on each other (see Table 1). For the targeted application, the magnetic gap thickness is rather large in the range of 4 to 8% of the overall motor radius, because the sealed chamber has to be installed through this gap. Finally, for the stator, the radial thickness of the tooth tip δ_{tt} has to be chosen (see section 3). The remaining (non-radial) geometric parameters determine the motor height (or length, respectively) l and the geometric shape of the stator teeth. Table 1 gives an overview of the considered design variables. In order to allow for scalable design considerations, the geometric variables are set in relation to two independent variables, namely the outer rotor radius r_R and the magnet angle α_{PM} . (The latter is actually given once the pole pair number was chosen). The remaining geometric variables can then be expressed as a fraction of these two independent variables, with factors f (where $0 < f < 1$) and n (where $n > 0$).

Apart from the geometric variables, there is one more important design parameter, namely the maximum allowed current density J_{max} in the stator coils. It can be chosen independently of the geometric variables. However, it is influenced by the temperature ratings of the motor and depends on the material choice and the cooling effort (e.g. conventional air cooling or more complex water cooling). The magnetomotive force, which determines the producible forces, results from the available winding area A_{coil} and the maximum allowed current density J_{max} .

$$\Theta_{\max} = J_{\max} \cdot A_{\text{coil}}. \quad (1)$$

The winding area itself is a function of several design parameters

$$A_{\text{coil}} = f(q, r_S, \delta_{\text{tt}}, \alpha_t). \quad (2)$$

For the optimization of the torque and the radial bearing forces (for fixed outer motor dimensions), this maximum allowed current density has to be set as a boundary condition. Moreover, the required magnetic gap thickness has to be determined. It is usually derived from the required application specifications. Additionally, the saturation curve of the iron material has an influence, because an energy-dense design with large magnetomotive forces can only be achieved when the iron parts are slightly driven into saturation. However, there is an upper limit, because the rotor performance would be reduced drastically for too extensive saturation values. For the remaining design variables, there is mutual interdependence because of these boundary conditions. For higher magnetomotive force (influenced with the winding area for fixed J_{\max} or the permanent magnet thickness), the iron parts have to be enlarged in order to avoid heavy saturation. The enlargement of the iron parts however, leads to a reduction of the available space for windings and permanent magnet material and it reduces the magnetic gap radius. In the end, an optimal design, where the proportion of iron, winding, and permanent magnet material is well balanced, can be found. Unfortunately, this setup is only valid if the boundary conditions (maximum allowed current density, magnetic gap thickness and iron material) stay constant. If there is a change in one of these factors, the optimum has to be determined again.

There are other important design parameters, such as material choice or coil layout (e.g. winding number, shape, and wire diameter). Moreover, the electrical ratings (required power, system voltage and maximum possible current) have to be chosen at an early design step.

TABLE I. DESIGN PARAMETER

Parameter	Symbol	Normalized value
Stator slot number	q	
Pole pair number	p	$[f(q)]^a$
Outer rotor diameter	r_R	
Maximum allowed current density	J_{\max}	
Permanent magnet angle	α_{PM}	$[360^\circ / 2p]$
Magnetic gap thickness	δ_m	$f_m = \delta_m / r_R$
Permanent magnet thickness	δ_{PM}	$f_{\text{PM}} = \delta_{\text{PM}} / r_R$
Back iron thickness	δ_{BI}	$f_{\text{BI}} = \delta_{\text{BI}} / r_R$
Stator tooth angle	α_t	$n_t = \alpha_t / \alpha_{\text{PM}}$
Tooth tip angle	α_{tt}	$n_{\text{tt}} = \alpha_{\text{tt}} / \alpha_{\text{PM}}$
Tooth tip thickness	δ_{tt}	$f_{\text{tt}} = \delta_{\text{tt}} / r_R$
Motor height	l	$n_l = l / r_R$
Stator radius	r_S	$[r_R - (\delta_{\text{BI}} + \delta_{\text{PM}} + \delta_m)]$

a. The pole pair number is dependent on the slot number, because only certain pole/slot combinations are allowed for a bearingless motor construction [11].

III. DESIGN STUDY FOR THE STATOR TEETH

When looking at the design of the stator teeth together with the tooth tips, very interesting characteristics can be found. There are three main geometric variables that can be varied, namely the tooth angle α_t , the radial tooth tip length δ_{tt} and the tooth tip angle α_{tt} . Using 3D electromagnetic FEM simulations [13], the influence of the tooth shape on the torque and the passive and active bearing forces is investigated.

A. Influence on Torque

Fig. 3 shows the motor torque for three different normalized stator tooth angles [$n_t = 25\%$, 50% and 75% in (a), (b)

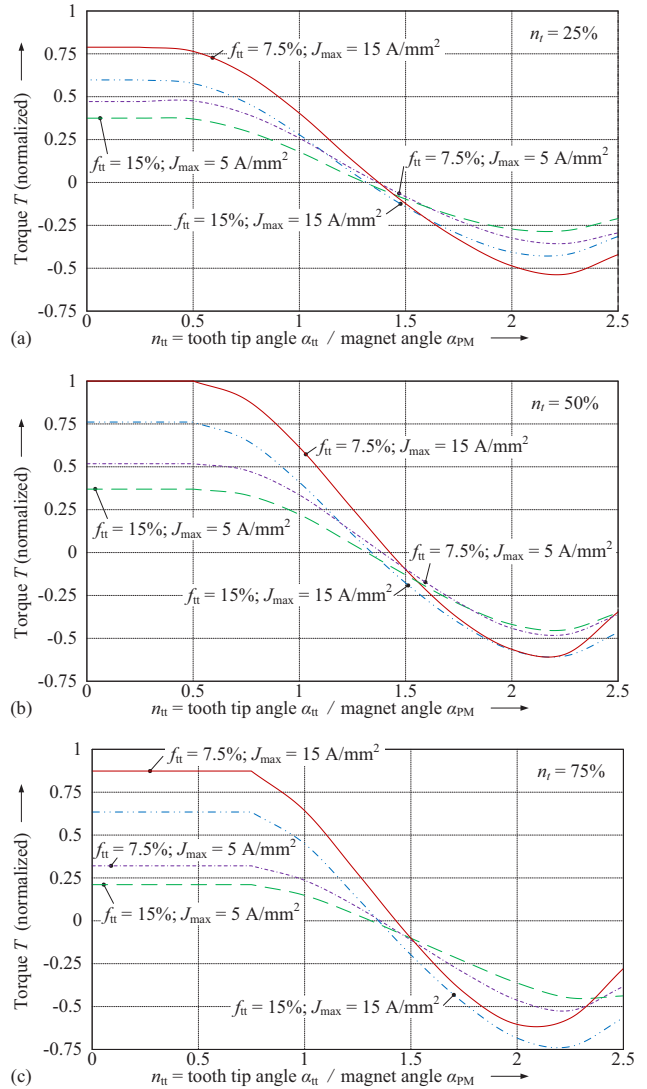


Figure 3. Influence of the tooth tip angle α_{tt} and the radial tooth tip length δ_{tt} on the torque for two different excitation levels ($J_{\max} = 5$ and 15 A/mm^2) and three different tooth angles [$n_t = 25\%$, 50% and 75% in (a), (b), and (c), respectively]. It can be seen that the torque reverses when the tooth tip angle is enlarged. Therefore, the tooth tip can either be built narrow (open tooth) or wide (closed tooth). The torque plots have been normalized with the highest torque value occurring in (b). Note that the design and consequently the torque remain constant for all $n_{\text{tt}} \leq n_t$. [$f_m = 6.75\%$, $f_{\text{PM}} = 8\%$ and $f_{\text{BI}} = 6.75\%$.]

and (c)] in dependence on the tooth tip thickness and the tooth tip angle. Moreover, the maximum allowed current density is varied between 5 A/mm^2 , which represents an application without any additional cooling (just ambient air), and 15 A/mm^2 , which represents an application with additional water cooling of the coils. When enlarging the tooth tip angle, the torque first decreases until it reaches zero and then reverses its direction. Therefore, two design options with either open teeth (small tooth tip angle) or closed teeth (large tooth tip angle) are possible for the generation of sufficient motor torque. Additionally, Fig. 3 reveals that there is an optimal tooth angle for open teeth in the range of 50% of the permanent magnet angle [as in (b)] and that the tooth tips should not exceed a certain thickness, whereas for closed teeth the tooth angle and the tooth tip thickness should be rather large [as in (c)].

B. Influence on Passive Bearing Forces

The possibility of choosing different ranges for the tooth tip angle is advantageous for the design of the passive magnetic bearing, because an important relation holds true for the attracting passive reluctance forces. When the tooth tip angle is increased, larger iron areas are facing the magnets. Consequently, all the passive forces get enlarged. For the axial and the tilting stability, larger reluctance forces are desirable because the bearing stability directly depends on them. In Fig. 4, the axial force action onto two joining magnets (one pole pair) in dependence on the angular rotor position is shown. For small tooth tip angles, there is a large difference whether the pole pair faces the center of a tooth tip (for rotor angles of 0° , 60° , ...) or whether it is in between two stator teeth (for rotor angles of 30° , 90° , ...). This

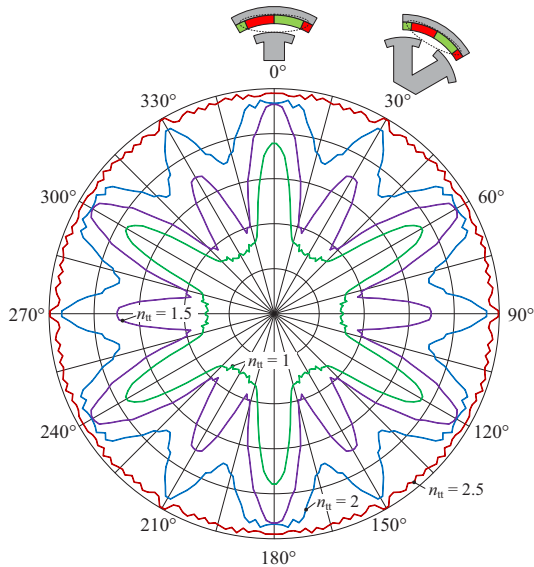


Figure 4. Influence of the tooth tip angle on the axial force (normalized) acting onto two joining magnet (one pole pair) of the rotor in dependence on the angular position. The force is larger when the magnet is exactly in front of a tooth tip (0° , 60° , etc.) than when it is in between two stator teeth (30° , 90° , etc.). However, this influence vanishes when the tooth tip angle is enlarged. Summed over all magnets, it is obvious that for larger tooth tip angles the total axial force acting on the rotor gets larger. [$n_t = 50\%$, forces are normalized.]

difference vanishes when the tooth tip angle is enlarged. For the overall axial force acting on the rotor (summed up over all magnets), this strong variation for small tooth tip angles smoothens out. Moreover, the total force is obviously larger with an increased tooth tip angle. There is an unavoidable trade-off between the desired large passive bearing forces in axial and tilting direction and the passive reluctance forces in radial directions. The latter pull the rotor out of its center position and an active control is required to bring the rotor back to the working position. This means that an active bearing has to counteract the destabilizing passive radial forces. In order to decrease the required effort for the active radial bearing, this destabilizing passive force should be small, which is in direct contradiction to the wish for large axial and tilting stability.

The mentioned influence of the tooth tip angle on the passive radial force is shown in Fig. 5. The rotor is displaced

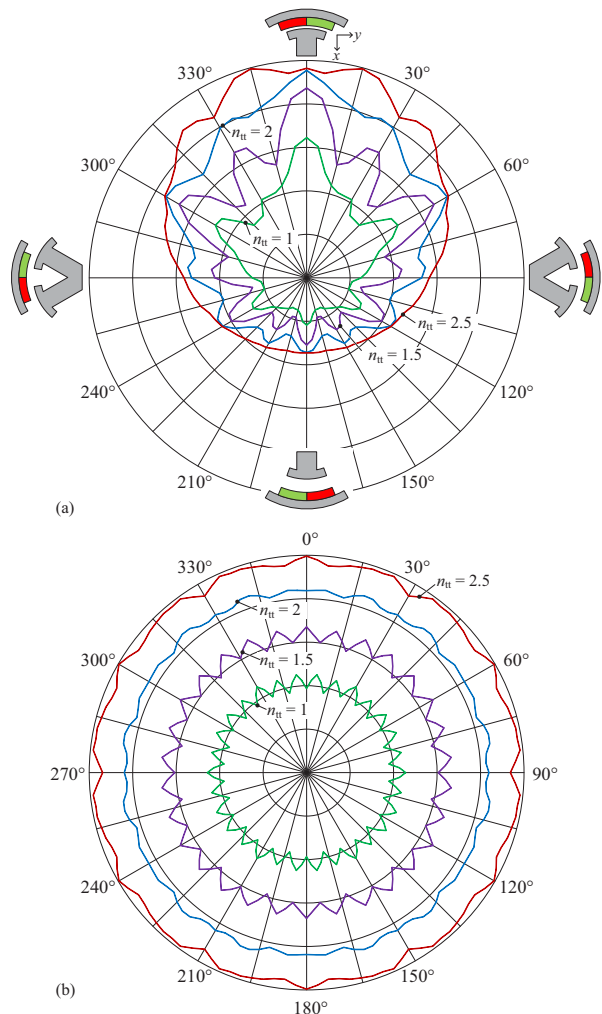


Figure 5. Destabilizing radial force acting onto two joining magnets (one pole pair) and the back iron ring in (a) and onto the rotor in (b) in dependence on the tooth tip angle and the angular rotor position. The rotor is displaced into the positive x -direction towards the junction of the considered pole pair for an angle of 0° . Summed up over all magnets, the total rotor becomes more or less independent of the angular position and it is enlarged along with the tooth tip angle. [$n_t = 50\%$, forces are normalized in (a) and (b) individually.]

from its center position changing the magnetic gap in dependence on the rotor angle. In Fig. 5(a), the attracting radial force acting onto these very two magnets (one pole pair, the remaining magnets have been omitted) and the back iron ring is plotted for varying rotor angles with the force measured in radial direction. The rotor displacement is constant (into the positive x -direction) so that the magnetic gap in between the stator and this magnet pair changes with the rotor angle. In the beginning (at 0°) the magnetic gap is narrow, then increases and becomes maximal for 180° . The curve would describe a circle if there was no radial displacement (i.e. no change in magnetic gap). In this case however, the curve is distorted, as can be seen in Fig. 5(a). Additionally, it can be seen that the forces grow with increased tooth tip angles. Summing up over all rotor magnets, the resulting radial force becomes more or less independent from the rotor angle [see Fig. 5(b), normalized after a rotor displacement into the positive x -direction]. Obviously, the total force also becomes larger once the tooth tips are enlarged. From this point of view, smaller tooth tips would be favorable for the radial bearing, as discussed before.

C. Influence on Active Radial Bearing

It was shown that the passive radial forces are enlarged when the tooth tip angle is increased. Therefore, it has to be investigated whether the active magnetic bearing in radial direction can counteract these forces in order to guarantee a stable operation. In Fig. 6(a), the resulting radial force for different radial rotor displacements into the negative x -direction in dependence on the tooth tip angle is shown. Due to stator and rotor encapsulations and the tank wall in between the magnetic gap, the actual fluid gap (which is the operating range that has to be controlled by the bearing) is about 40% of the magnetic gap. If no current is applied to the coils, a negative force results which would displace the rotor even further until it comes to a mechanical touchdown (curve I). Hence, a counterforce (II) has to be generated with the coil system so that the overall force becomes positive again and moves the rotor back into the positive x -direction towards its center position (III and IV). Fig. 6(a) further reveals that the rotor can be stabilized for $n_{tt} < 65\%$ in case of low excitation with 5 A/mm^2 or up to $n_{tt} < 110\%$ if high excitation (15 A/mm^2) is applied.

For larger tooth tip angles (beyond 150%), the active radial force (II) is reversed for the same excitation (similar to the torque) and the bearing would just support the displacement instead of counteracting it. Therefore, the excitation has been reversed in Fig. 6(b) for closed stator teeth. It can be seen that the active force (II) becomes positive and it is counteracting the destabilizing passive one (I). However, the resulting total force (III and IV) never becomes positive which means that the destabilizing passive radial force is dominant even for a displacement of only 20%. Moreover, even for high excitation (IV, with 15 A/mm^2), the active bearing cannot cope with the destabilization. In fact, the difference between moderate excitation (III, with 5 A/mm^2) compared to high excitation is

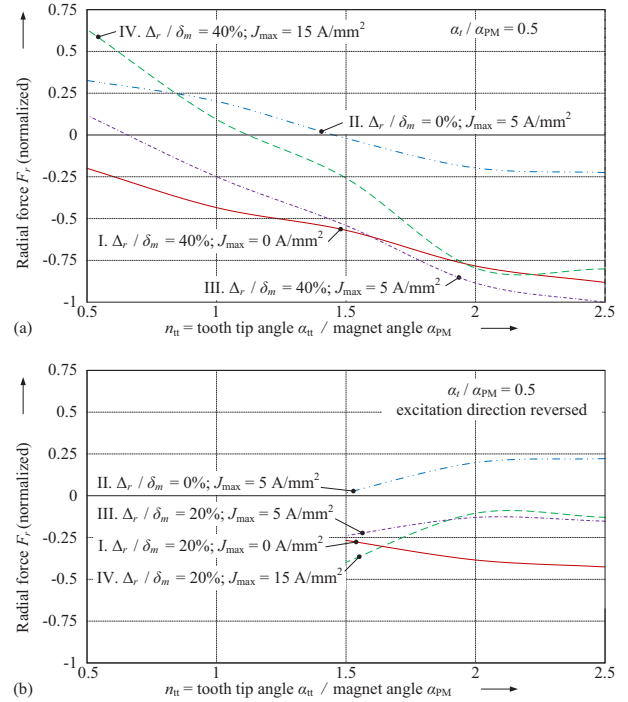


Figure 6. Active and passive radial bearing forces in dependence on the tooth tip angle. A radial displacement into the negative x -direction leads to a negative radial force. In the case of open stator teeth, the active bearing force can counteract this destabilizing force and bring the displaced rotor back to its center position (a). For closed teeth however, the passive force is dominant and the rotor position is not controllable anymore even with high excitation currents (b). [$f_m = 6.75\%$, $f_{PM} = 8\%$, $f_{BI} = 6.75\%$ and $f_{tt} = 7.5\%$.]

very small which means that there is almost no gain anymore for the active force when the excitation is increased. This is an indicator that the iron material is heavily driven into saturation. As in the case of the torque, the tooth tip thickness δ_{tt} could be enlarged to decrease the saturation level. However, this also decreases the available winding area and, consequently, the applicable magnetomotive force.

D. Open Versus Closed Teeth

In the previous sections, it was found that there generally exist two possibilities to design the stator teeth. They can either be open, with the tooth tip angle in the range of the tooth angle itself, or closed with rather large tooth tip angles. Both alternatives could produce sufficient torque, whereas closed teeth would be beneficial for the passive magnetic bearing. For the active magnetic bearing however, a stable implementation with closed teeth is hardly achievable for the required working range. Therefore, a setup with open stator teeth has to be recommended for this type of bearingless motors and the intended applications. In order to decrease the system complexity, the tooth tips could even be omitted, leading to bar-shaped stator teeth. This measure would allow for less costly manufacturing of the stator and the coils and would simplify some of the assembly steps.

IV. VERIFICATION WITH TEST SETUP

A prototype setup has been realized in order to confirm the simulation results and to test the motor in a practical manner. The stator with the concentrated coils is depicted in Fig. 7(a). It can be seen that the tooth tips have been omitted, following the design considerations elaborated before. The stator and the sensor system (for radial and angular position measurements) are then placed below a stainless steel cup [see Fig. 7(b)]. This cup represents the tank indentation so that a real application situation can be tested. The rotor ring (back iron and permanent magnets) levitates around the buried motor.

A test run with an experimental tank setup has been undertaken and the corresponding measurements are presented in Fig. 8. In the beginning, the rotor (with mixing head) is levitated and turning with 100 rpm inside water. During the test, it is accelerated to 280 rpm and decelerated back to 100 rpm again. The radial positions (split into x - and y -direction) are permanently measured during the whole experiment. It can be seen that the radial rotor is kept in the center position with high accuracy during the whole test. Additionally, the drive and bearing current of one phase is determined. The latter reveals that only little current is needed for a stable control of the magnetic bearing. The drive current is rather small for the lower speed. Once it is running with 280 rpm however, the water flow becomes turbulent and a rather large torque is required to overcome the water resistance. Consequently, the current increases in order to provide the mixing torque.

V. CONCLUSION

A general design study for bearingless motors in exterior rotor construction has been presented. The important design parameters have been listed and their interconnections were explained. For the stator, it was shown that the teeth can either be open (small tooth tip angle) or closed (large tooth tip angle) for both torque and passive bearing forces. For the active radial bearing, however, a design implementation with open teeth is clearly recommended. Therefore, the suggestion is to omit the tooth tips and to use bar-shaped stator teeth.

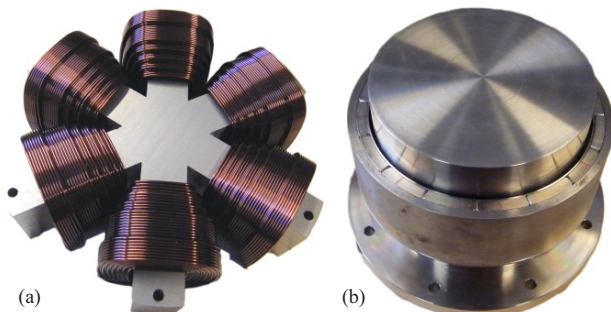


Figure 7. The stator in (a), which consists of six concentrated coils (one per stator tooth), is placed below a stainless steel cup in (b). For this prototype, the cup represents the tank indentation. The rotor ring is placed around the tank indentation (see also Fig. 1).

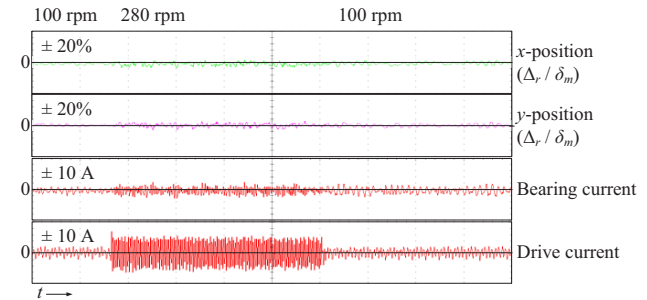


Figure 8. Measurements of the radial positions and the bearing and drive current in one phase using the prototype motor inside a test tank. The rotor is levitated and running with 100 rpm in water. The rotor current is small for the lower speed and increases when mixing with 280 rpm. The radial positions are controlled in a very stable manner during the whole experiment.

REFERENCES

- [1] T. Schneeberger, T. Nussbaumer, and J. W. Kolar, „Magnetically Levitated Homopolar Hollow-Shaft Motor,“ *IEEE/ASME Trans. Mechatronics*, vol. 15, no. 1, pp. 97–107, Feb. 2010.
- [2] W. Gruber, T. Nussbaumer, H. Grabner, and W. Amrhein, “Wide Air Gap and Large-Scale Bearingless Segment Motor With Six Stator Elements,” *IEEE Trans. Magn.*, vol. 46, no. 6, pp.2438–2441, Jun. 2010.
- [3] G. Catapano, P. Czermak, R. Eibl, D. Eibl, and R. Pörtner, “Bioreactor Design and Scale-Up,” in *Cell and Tissue Reaction Engineering: Principles and Practice*, 1st ed., vol. 1, Berlin Heidelberg: Springer-Verlag, pp. 173–259, 2009.
- [4] M. Ooshima, A. Chiba, T. Fukao, and M. A. Rahman, “Design and Analysis of Permanent Magnet-Type Bearingless Motors,” *IEEE Trans. Ind. Electron.*, vol. 43, no. 2, pp. 292–299, Apr. 1996.
- [5] S. Silber, W. Amrhein, P. Boesch, R. Schoeb, and N. Barletta, “Design aspects of bearingless slice motors,” *IEEE/ASME Trans. Mechatronics*, vol. 10, no. 6, pp. 611–617, Dec. 2005.
- [6] F. Zürcher, T. Nussbaumer, W. Gruber, and J. W. Kolar, “Design and Development of a 26-Pole and 24-Slot Bearingless Motor,” *IEEE Trans. Magn.*, vol. 45, no. 10, pp. 4594–4597, Oct. 2009.
- [7] M. Ooshima and C. Takeuchi, “Magnetic Suspension Performance of a Bearingless Brushless DC Motor for Small Liquid Pumps,” *IEEE Trans. Ind. Appl.*, vol. 47, no. 1, pp. 72–78, Jan. 2011.
- [8] W. Gruber, W. Amrhein, and M. Haslmayr, “Bearingless Segment Motor With Five Stator Elements: Design and Optimization,” *IEEE Trans. Ind. Appl.*, vol. 45, no. 4, pp. 1301–1308, Jul. 2009.
- [9] Y. Asano, A. Mizuguchi, M. Amada, J. Asama, A. Chiba, M. Ooshima, M. Takemoto, T. Fukao, O. Ichikawa, and D. G. Dorrell, “Development of a Four-Axis Actively Controlled Consequent-Pole-Type Bearingless Motor,” *IEEE Trans. Ind. Appl.*, vol. 45, no. 4, pp. 1378–1386, Jul. 2009.
- [10] Y. Christi and M. Moo-Young, “Clean-in-place systems for industrial bioreactors: Design, validation and operation,” *Journal of Industrial Microbiology and Biotechnology*, vol. 13, no. 4, pp. 201–207, Jul. 1994.
- [11] T. Reichert, T. Nussbaumer, W. Gruber, and J. W. Kolar, “Bearingless Permanent-Magnet Motor with 4/12 Slot-Pole Ratio for Bioreactor Stirring Applications,” *IEEE/ASME Trans. Mechatronics*, vol. 16, no. 3, pp. 431–439, Jun. 2011.
- [12] T. Reichert, T. Nussbaumer, and J. W. Kolar “Novel Bearingless Brushless Motor in Exterior Rotor Construction for Stirred Bioreactors,” *5th IET International Conference on Power Electronics, Machines, and Drives, PEMD 2010*, Apr. 2010.
- [13] Ansoft. Corp. (Pittsburgh, Pennsylvania), „Maxwell 3D,“ 2011, available at: <http://ansoft.com/products/em/maxwell/>.